To evaluate OKR adaptation, the mean OKR gain was plotted for each 10-min interval (Figure 2C). Saline-injected normal mice (control) exhibited a time-dependent increase in the OKR gain, but no gain increase was observed in the mutant or the memantine-treated normal mice.

Figure 2. The optokinetic response (OKR) and its susceptibility to memantine. (**A**) The OKR of normal and mutant mice after intraperitoneal injection of saline (control) or memantine-containing saline (10 mg/kg). Measurements commenced 10 min after injection. Representative OKRs from normal and mutant mice are shown. The relative pupil azimuth is plotted against time. Each trace indicates the average over each 10-min period of a 1-h measurement session. Screen, movement of the stimulus screen; (**B**) Overall OKR gain throughout the 1-h session with or without memantine. Dots and error bars, mean ± SD; n = 5 for each data point. * $p < 0.05$, ** $p < 0.01$, and **** $p < 0.0001$, multivariate ANOVA. The overall OKR gain was calculated by averaging the OKR gains for all 10-min periods in a single 1-h session (see panel C); (**C**) Time course of the mean OKR gain for normal (n = 5) and mutant (n = 5) mice. Each dot indicates the average over a 10-min period of a 1-h measurement session. Error bars indicate ±SD. **** $p < 0.0001$ *vs.* the control for time × drug interaction, repeated measures ANOVA.

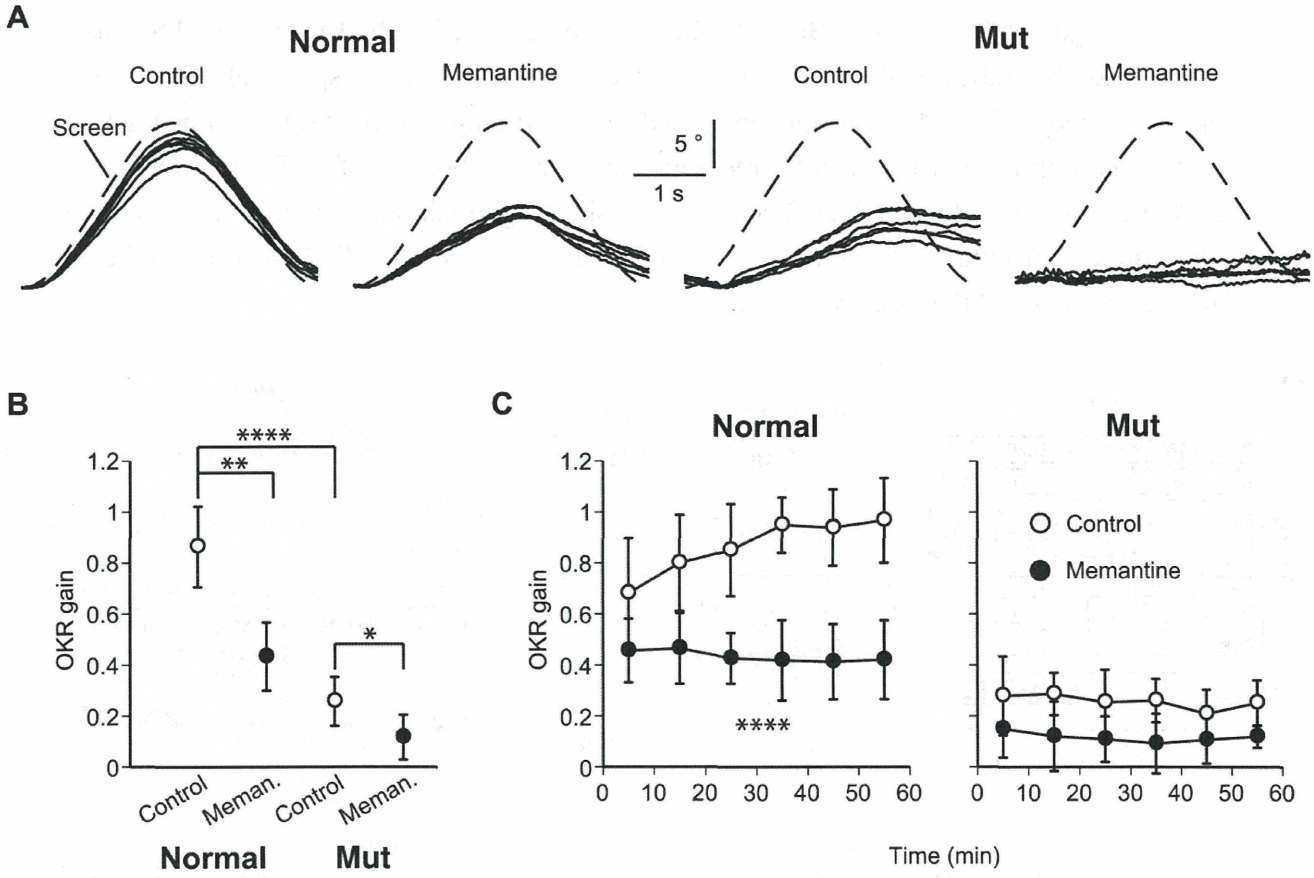

2.3. Microsatellite Analysis in the Ataxic Mice

Because the pharmacological analyses were unable to predict the gene responsible for the ataxic phenotype, we performed a microsatellite analysis to identify the gene. Sperm were isolated from an ataxic mouse (N0: C57BL/6J[B6], B6/B6) and used to perform IVF with oocytes from C3H/HeN (C3) mice (normal: C3/C3). Oocytes were prepared from the N1 female (B6/C3 hetero-mice) and used for a second round of IVF using the original sperm from the N0 (B6/B6) ataxic mice, which produced 137 N2 mice (75 non-ataxic (the responsible genomic-region should be B6/C3) and 62 ataxic (the responsible genomic-region should be B6/B6)). Using 60 microsatellite markers and DNA from eight N2 non-ataxic mice, we screened heterogenic-regions composed of both B6 and C3 chromosomes. We observed that D6Mit149 (Chromosome 6, 48.93 cM) was amplified as the heterogenic-type in all eight mice. Next, we analyzed other markers near D6Mit149 using DNA from 70 mice (Figure 3A) and narrowed the responsible region to 27.3–32.2 cM (D6Mit384–D6Mit243), which was also associated with the phenotype of enhanced memantine susceptibility.

Figure 3. Identification of the responsible gene. (**A**) Microsatellite analyses of N2 mice. B6, parental allele of the ataxic mouse (C56BL/6J); C3, WT allele of C3H/HeN. N2 mice were produced following *in vitro* fertilization with oocytes from hetero N1 (B6/C3) and sperm from the original N0 ataxic B6 (B6/B6). Markers are described in the Experimental Section. Normal and Mut indicate mice with or without the ataxic phenotype, respectively. The *Grid2* gene is located 29.77 cM in chromosome 6; (**B**) The full-length open reading frame ORF of *Grid2* was amplified from cDNA prepared from the cerebellum of WT and Mut mice; (**C**) Western blotting for GRID2; (**D**) A diagram showing break points in the *Grid2* gene of ataxic mice; (**E**) Putative protein sequence of GRID2 in *Grid2*$^{Htake/Htake}$ mice is predicted from diagram D and the direct ORF sequence.

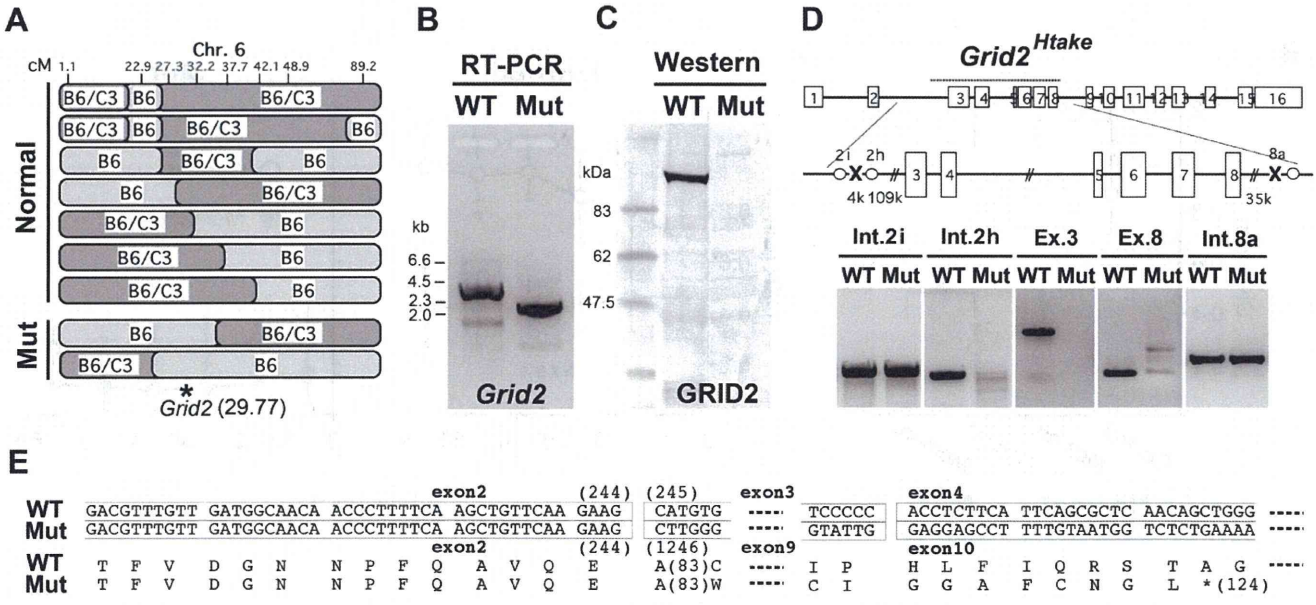

When we searched for genes that have known associations with ataxic phenotypes, we noticed the *Grid2* gene at 29.77 cM [30]. To determine whether this gene was responsible for the observed

phenotype, the *Grid2* open reading frame (ORF) was amplified from cDNA prepared from the cerebellum. As shown in Figure 3B, the *Grid2* ORF was approximately 1 kb shorter in the mutant mice than in the WT mice. In addition, western blotting for GRID2 revealed that this protein was absent from the mutant cerebellum (Figure 3C).

Direct sequencing of the mutant ORF suggested that the region from exon 3 to exon 8 might be deleted, which is the longest deletion reported in *Grid2* mutant mice [31]. Chromosome walking (Figure 3D) identified the break points 110 kb upstream from exon 3 and 30 kb downstream from exon 8, which yielded a truncated GRID2 protein similar to that in the $Grid2^{trp/trp}$, $Grid2^{ho8J/ho8J}$, and $Grid2^{ho13J/ho13J}$ mutants, but with different flanking peptides (Figure 3E). Our laboratory code for mutant mouse lines is Htake, thus the mutant allele is named $Grid2^{Htake}$.

2.4. Altered Sensitivity to NMDA in Cultured Granule Cells of $Grid2^{Htake/Htake}$ Mice

GRID2 is highly expressed in Purkinje cells, and disruption of GRID2 signaling impairs Purkinje cell functions. However, little or no expression of functional NMDA receptors in Purkinje cells of the adult cerebellum has been reported [32]. Thus, it is possible that *Grid2* gene deletion influences cerebellar function by affecting NMDA receptors on granule cells. We examined whether $Grid2^{Htake/Htake}$ mice possessed memantine-sensitive NMDA receptors on cerebellar granule cells, using granule cell-enriched (Purkinje cell-free) primary cultures from P2 mice. Quantitative PCR (Figure 4A) and western blot analyses (Figure 4B) showed that cultured granule cells expressed low, but detectable, levels of *Grid2* mRNA and GRID2 protein. No significant difference in NMDAR1 protein level was observed between the cultures derived from normal and $Grid2^{Htake/Htake}$ mice, which was consistent with the result of mRNA (microarray) analyses (Supplementary Table S1).

We have to note, however, that no significant interaction between GRID2 protein and NMDAR1 protein in the total cerebella or cultured granule cell lysate was observed (Supplementary Figure S2), despite the presence of PKC gamma binding to GRID2 protein [33].

Next, we monitored NMDA-induced currents in cultured granule cells using a whole-cell voltage-clamp technique. At cell densities as low as 1.25 million cells/mL and a holding potential of −90 mV, granule cells from both WT and mutant mice showed no baseline activity (Figure 4C). In the absence of memantine (before memantine), NMDA (20 μM, 2 s) induced inward currents that were larger in WT cells than in mutant cells. Furthermore, NMDA-induced currents were reduced in the presence of memantine (after memantine: 10 μM, 30 s). However, the magnitude of the memantine-dependent suppression of the NMDA-induced currents varied in the individual cells.

To accurately categorize the memantine-sensitive NMDA-induced currents, we divided the cells into two categories based on the ability of memantine to reduce the charge density of NMDA-induced currents by more than 75%. According to this classification, 51.9% of WT cells and only 21.4% of mutant cells were categorized as memantine-sensitive (Figure 4D). Moreover, the classification (only open circles) revealed that the values of charge density from the mutant cells fell into a lower range, which produced a significant difference in the variance of the charge density between the WT and mutant groups (Figure 4E). These results suggest that mutant mice might possess a poor variation of NMDA receptor with reduced function on their granule cell population.

Figure 4. NMDA-responsiveness of cultured cerebellar granule cells. (**A**) The raw data for quantitative PCR analyses and normalized levels (inset: n = 4) of *Gird2* mRNA are indicated. Total RNA was prepared from total cerebellum, 2-week-cultured cerebellar granule cells from neonates (P2), B16F10 melanoma cells (non-neuronal negative control); (**B**) Western blotting was performed using WT and *Grid2*$^{Htake/Htake}$ (Mut) total cerebella or cultured granule cells. There is no significant difference in NMDAR1 protein level; (**C**) Whole-cell current responses of cultured granule cells derived from WT and Mut mice to local application of NMDA (20 μM, 2 s) before and after treatment with memantine (10 μM, 30 s). Representative currents recorded from single WT and Mut cells. Arrowheads indicate artifacts due to the opening and closure of the electromagnetic valve controlling delivery of NMDA-containing saline; (**D**) The examined cells were categorized into two groups by memantine susceptibility, and their populations are represented as % fractions. When more than 75% of NMDA-induced inward current was suppressed by memantine, the cells were categorized into the memantine-sensitive group (white area). Cells that experienced reduced inward current suppression after memantine treatment, or no significant inward current were categorized into the memantine-insensitive group (black area). * $p = 0.0178$, likelihood ratio test (WT, n = 27; Mut, n = 28); (**E**) Distribution of the total charge density of NMDA-induced inward currents. Open circles (white) and closed triangles (black) indicate the data from cells categorized as D. The magnitude of the total data (white and black) was not significantly different between the WT and mutant cells (medians, 1.01 and 0.64 pC/pF, respectively). However, in a comparison of the data from the memantine-sensitive cells (white), there was a significant difference in variance between the WT and mutant cells (* $p = 0.0120$, Brown-Forsythe test).

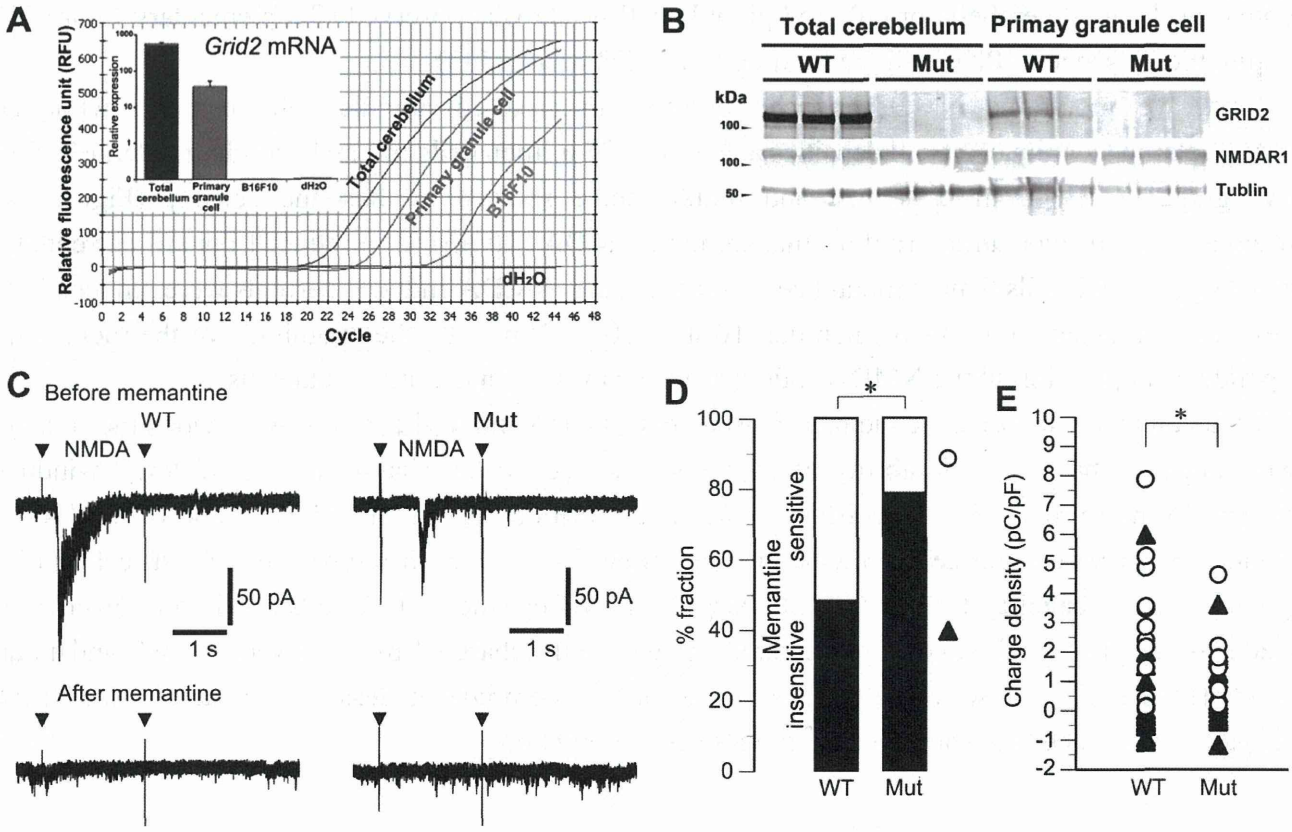

2.5. Mice Treated with Memantine and AMPA Were Unable to Walk Smoothly

GRID2 deficiency results in dysregulation of AMPA receptors [34,35]. To examine whether impaired AMPA receptor functions affected memantine susceptibility, mice were treated with memantine simultaneously with the AMPA receptor agonist AMPA or the antagonist DNQX [36], and the movements of these mice were monitored (Figure 5A). The mice treated with AMPA (20 mg/kg) walked slowly and sometimes crouched on the floor. However, mice treated with both memantine (10 mg/kg) and AMPA had increased activity and did not stop walking. In addition to these abnormal behaviors, the mice walked with a mild staggering gait and sometimes slipped (roll-over: Figure 5B, Supplementary Movie 4). These combined effects of memantine on mouse behavior were not observed when memantine was administered with DNQX (10 mg/kg), although the mice treated with DNQX were also sometimes crouched. Moreover, in the *Grid2*$^{Htake/Htake}$ mice, co-treatment with AMPA and a low dose of memantine (5 mg/kg) caused more evident balance impairment than memantine treatment alone (Supplementary Figure S3), suggesting that GRID2 deficiency may augment the synergistic action of AMPA and memantine. The effect of AMPA co-treatment could not be evaluated with a higher dose of memantine (10 mg/kg) because the maximal effect was induced by this dose of memantine.

Figure 5. Effect of AMPA receptor modulators on memantine action in WT mice. (**A**) Monitoring of walking mice (12-week-old WT male, n = 6) after memantine treatment (10 mg/kg) combined with AMPA (20 mg/kg) or the AMPA receptor antagonist DNQX (10 mg/kg). Ten minutes after the treatments, the walking distance for 5 min was expressed as the mean and SD, * $p < 0.05$ *vs.* the other conditions (unpaired *t*-test; $p < 0.0001$ for overall differences, one-way ANOVA); (**B**) Number of rollovers in 5 min was counted. NO indicates that rollover was not observed. n = 6 for Control and AMPA + memantine and n = 3 for the other conditions. The occurrence of rollover was significantly different between AMPA + memantine and the other conditions ($p < 0.05$, Fisher's exact test); (**C**) OKRs measured in female WT mice with sequential injections of the control saline, AMPA (10 mg/kg), or DNQX (5 mg/kg) and memantine (5 mg/kg). A set of traces indicates representative responses of individual mice. Dotted line, the movement of the stimulus screen; (**D**) Graph shows the mean and ±SD of OKR gain (n = 3 for each condition). *p* value (without a bracket, one-tailed unpaired *t*-test; with brackets, paired *t*-test) is indicated when significance was observed.

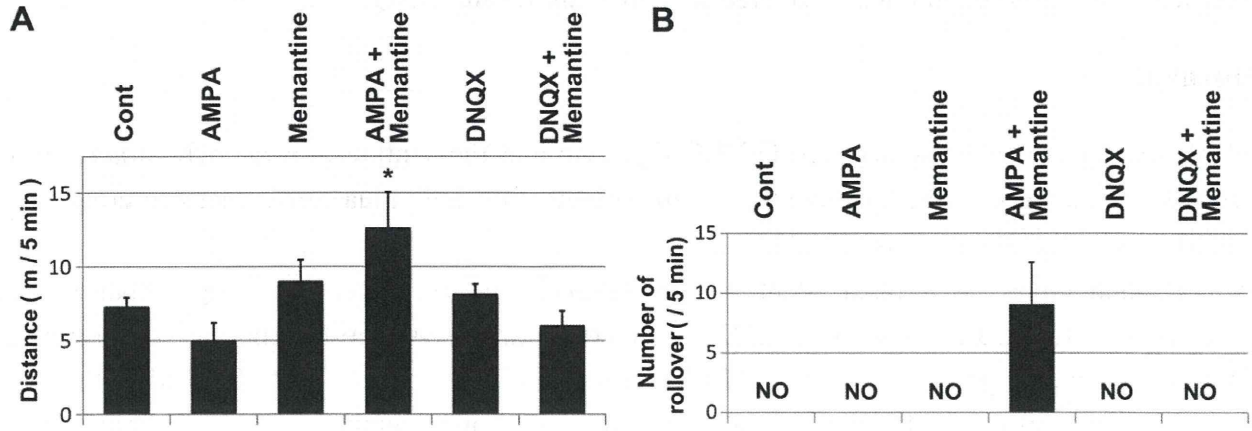

Figure 5. *Cont.*

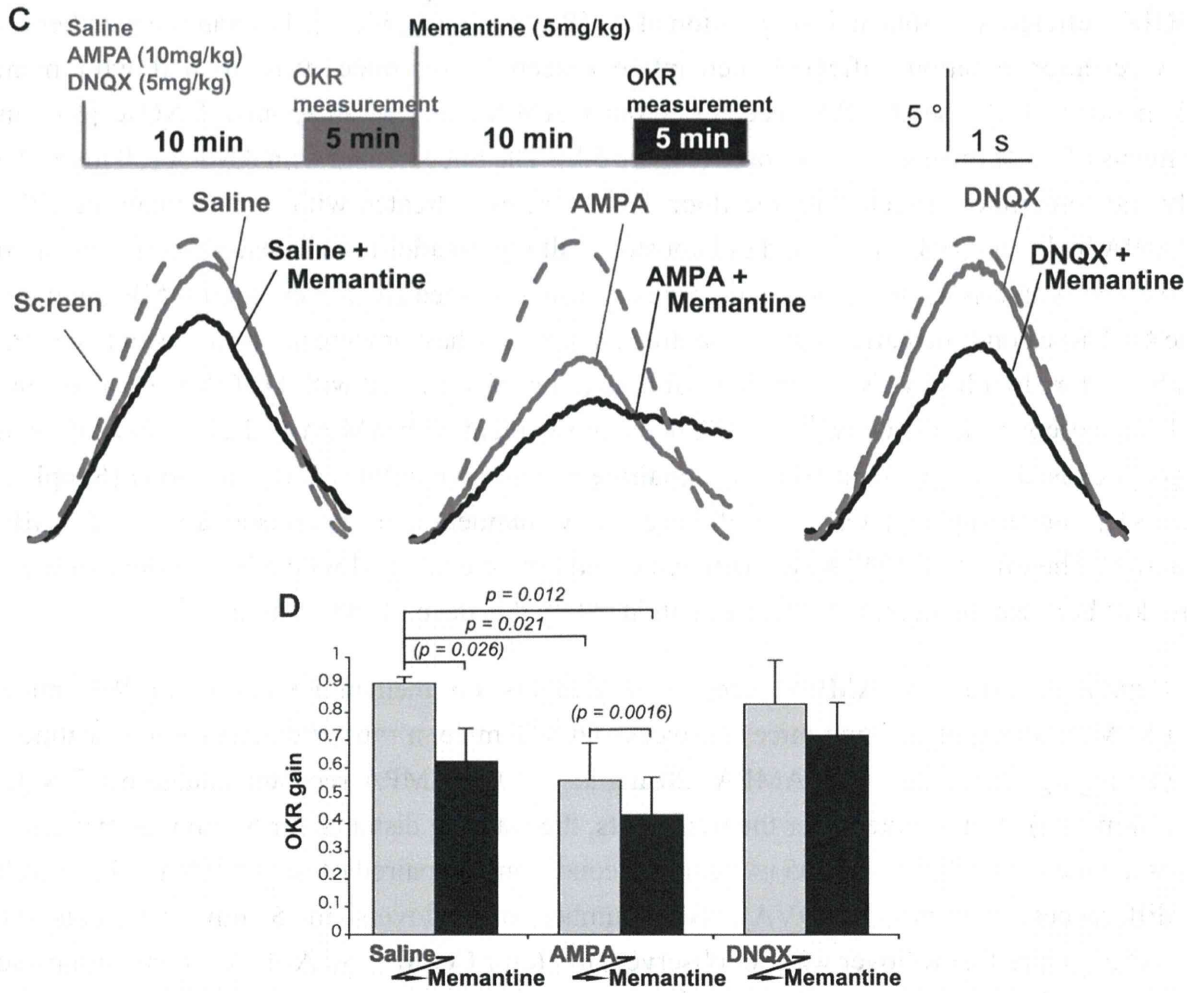

Finally, the OKR was monitored after co-treatment with memantine and AMPA or DNQX (Figure 5C). Mice were first treated with AMPA, DNQX, or saline, and the OKR was subsequently monitored for 5 min (because some mice closed their eyes after treatment with higher doses, AMPA (10 mg/kg) and DNQX (5 m/kg) were used for OKR measurement). To evaluate synergies between memantine and AMPA receptor modulators, the mice were further treated with a low dose of memantine (5 mg/kg), and again subjected to OKR measurements for another 5 min. AMPA significantly impaired the OKR, and the combined treatment with memantine further impaired the OKR (Figure 5D). These effects were not observed in mice co-treated with memantine and DNQX.

3. Discussion

Here, we report cross-talk between GRID2 signaling and memantine in mice, which may, in part, account for the adverse effects of memantine in patients with individual differences in congenital or acquired genetic factors, such as GRID2.

Major phenotypes have been identified in GRID2 mutant mice, including impaired motor coordination, learning, and memory. GRID2 is located on the postsynaptic membrane of Purkinje cells and binds to cerebellin precursor protein 1 (CBLN1) and neurexin 1 beta (NRXN1b) [7,8] on the parallel fibers of granule cells [7,37]. On the other hand, the memantine target, NMDA receptors, are also

expressed on the developing [38] and adult [39] cerebellar granule cells. Furthermore, contrary to the neurotoxic effects of glutamate, NMDA receptors were found to promote the survival of cultured Purkinje [40] and granule cells [41,42]. However, double-KO mice with disrupted *Nr2A* and *Nr2C* genes (encoding two major NMDA receptor subunits in the adult mice cerebellum) demonstrate a mild impairment in motor coordination, but they do not exhibit an ataxic phenotype [43]. This observation suggests that NMDA receptors and GRID2 functions may not be directly linked [44].

Thus, in the present study, pharmaco-behavioral approaches failed to identify *Grid2* as a candidate for the cause of the observed phenotypes. Unexpectedly, our efforts resulted in the observation of new phenotypes in our *Grid2* deficient mice, which appeared as enhanced memantine susceptibility, which was likely mediated by dysfunctional NMDA receptors [1,2,45]. OKR measurements in $Grid2^{Htake/Htake}$ mice revealed impaired basal cerebellar functions in eye movement, which was also mimicked by memantine treatment. Dizziness has been reported as a major adverse effect of memantine treatment in humans [6,46]. The cerebellar flocculus is thought to be responsible for the early stage formation of OKR adaptation and its memory [47,48].

The *Grid2* gene is located in a hot spot of genomic deletions [31], and a number of mutant lines with defects in this gene have been identified. In addition to naturally occurring mutants, targeted disruption and knock-in mutations of *Grid2* have been reported [30,49,50]. In contrast to these loss-of-function mutations, $Grid2^{Lc}$ (*Lurcher*) [51] was identified as a spontaneous dominant mutation characterized by cerebellar ataxia and atrophy of Purkinje and granule cells [30]. Physiological studies of $Grid2^{Lc/+}$ mice have shown that the $Grid2^{Lc}$ mutation produces constitutive inward Ca^{2+}/Na^{+} currents that induce cell death [52].

The importance of the genetic background on $Grid2^{Lc/+}$ mice phenotypes was also reported [47,53]. In congenic $Grid2^{Lc/+}$ mice, almost 99.99% of those on a C57BL/6 genetic background lost Purkinje cells, whereas no Purkinje cell loss was observed in $Grid2^{Lc/+}$ mice on a 93% C57BL/6 genetic background, indicating that phenotypes in $Grid2^{Lc/+}$ mice are highly dependent on their genetic backgrounds. Interestingly, abnormal eye-movement and impaired motor-coordination were only observed in 93% of C57BL/6 background-$Grid2^{Lc/+}$ mice possessing Purkinje cells, but not in 99.99% of C57BL/6 background-$Grid2^{Lc/+}$ mice without Purkinje cells [47], suggesting that gain of GRID2 signaling is also a cause of motor deficits in the presence of Purkinje cells. In contrast to $Grid2^{Lc/+}$ mice, we noticed during gene mapping that memantine-induced balance impairment was observed in $Grid2^{Htake/Htake}$ mice irrespective of their genetic backgrounds (mixed B6 and C3 backgrounds). This is also the case for random eye movements commonly observed in different *Grid2*-deleted mice with different genetic backgrounds, *Grid2*-KO in C57BL/6 and $Grid2^{ho\text{-}15J/15J}$ on a C3HJ background [17], suggested that memantine-induced balance impairment may occur in other *Grid2* deficient mice irrespective of their genetic backgrounds.

How does the $Grid2^{Htake}$ deletion enhance the actions of memantine? GRID2 regulates long-term depression (LTD) at synapses between immature parallel fibers and Purkinje cells by inducing AMPA receptor endocytosis [34,35]. D-Serine is an endogenous ligand for GRID2 and one of the factors that induce LTD [9]. Developing mice that express GRID2 with a disrupted D-serine binding site show impaired motor coordination and learning, suggesting the importance of LTD for motor regulation. On the other hand, NMDA receptor activation requires the removal of Mg^{2+} block, which occurs when the membrane potential increases through activation of non-NMDA receptors including AMPA receptors [4].

Cooperative signal-transmission from cerebellar mossy fiber-granule cells to Purkinje cells mediated by NMDA and AMPA receptors has been shown in both Mg^{2+} block dependent and independent manners [54]. We observed that co-treatment with memantine and AMPA impaired gait and OKR in wild type mice, suggesting that dysregulation of AMPA receptor function in *Grid2* deficient mice may cause the enhanced memantine susceptibility. This may be implicated in the decreased number of memantine-sensitive NMDA-responsible granule cells in *Grid2*$^{Htake/Htake}$ mice.

Whilst mapping the gene responsible for the ataxic phenotype, we observed new phenotypes in *Grid2* deficient mice, which were latent balance defects, and OKR impairments. These deficits were also mimicked by memantine with AMPA in the impaired WT mice. Because, recently, the wide distributions of *Grid2* mRNA and GRID2 protein were reported in the adult rodent brain [55], the phenotypes in *Grid2*$^{Htake/Htake}$ mice could be ascribed to not only attenuated NMDA receptor responsiveness in a subset of granule cells but also other cellular mechanisms.

When granule cells are collectively activated *in vivo*, glutamate spilt over from parallel fiber-Purkinje cell synapses stimulate adjacent interneurons (volume transmission), which in turn exert inhibition of Purkinje cells [44,56–58] crucial for normal motor coordination [59]. The GRID2 mutation may reduce NMDA receptor-mediated excitation of granule cells, and this might decrease the volume transmission and Purkinje cell inhibition via interneurons. Moreover, cerebellar interneurons (basket, stellate, and Golgi cells) also express functional NMDA receptors at their presynaptic membrane [44,56–58] and these receptors could be affected by the change of GRID2 signaling. Taken as a whole, the present study using a naturally occurring *Grid2* deleted mouse line may lead to a better understanding of NMDA, AMPA, and GRID2 receptors. Further studies are required to elucidate the precise mechanisms underlying GRID2 signaling.

4. Experimental Section

4.1. Animals

C57BL/6J (B6) and C3H/HeN (C3) from SLC Japan (Shizuoka, JAPAN) were used for the maintenance of the *Grid2*$^{Htake/Htake}$ mouse line and for IVF for microsatellite analyses, respectively. IVF was performed following a standard method [60] using human tubal fluid medium (Ark Resource, Kumamoto, Japan). The *Grid2* mutant mice, *Grid2*$^{Htake/Htake}$ (formal name is *Grid2*$^{ho\text{-}Htake}$/Nibio), were supplied by the JCRB Laboratory Animal Resource Bank at the National Institute of Biomedical Innovation. The experimental mouse protocols were approved by the Ethics Committee at the National Institute of Biomedical Innovation (assigned No. DS-23-35), and by the University of Toyama's Committee on Animal Experiments (assigned No. A2012eng-8) for animal welfare. For microarray analyses, cerebella were dissected after anesthesia of mice with isoflurane (WAKO Pure Chemicals, Osaka, JAPAN). The animals were maintained under standard light (08:00–20:00) and temperature conditions (23 °C, 50% humidity).

4.2. Reagents

Microsatellite markers were used to identify the chromosomal region responsible for the ataxic phenotype, (D6Mit86, 1.18 cM; D6Mit351, 22.94 cM; D6Mit384, 27.38 cM; D6Mit243, 32.2 cM 7;

D6Mit29, 37.75 cM; D6Mit102. 42.11 cM; D6Mit149, 48.93 cM; D6Mit200, 89.28 cM). To map the end points of the *Grid2* deletion, we used following primers: m*Grid2* intron 2H F 5'-GCT ACT TTG GTA CAA GTG GAC A and m*Grid2* intron 2H R 5'-GAC AAG TTG CTC TCT GTA TCT; m*Grid2* Intron 2I F 5'-CAT GCT CAC ATC AAA ATA CAT CAA and m*Grid2* Intron 2I R 5'-TGT AAT TGA GGAA AAT ACA TAA T. Other primers used in Figure 3D were prepared with reference to [31]. To identify the *Grid2* deletion in *Grid2*$^{Htake/Htake}$ mice, we used the following primers for PCR amplification: m*Grid2* Intron 2HIF 5'-TGG ATC CTT CTA CGT GCA AC, m*Grid2* Intron 8YF2 5'-GGA CCA CAC TGA GGT TCG AAA GA, and m*Grid2* Intron 8YR 5'-ATC TCT TGG CAT GCA TTA GAC. The mutant allele of *Grid2*^{Htake} produces a PCR band corresponding to a product of approximately 600 bp, and that for the WT allele is approximately 400 bp.

GRID2 antibody was obtained from Santa Cruz Biotechnology (Santa Cruz, CA, USA). Antibodies for NMDAR1 and tubulin were obtained from Cell Signaling Technology (Boston, MA, USA). Memantine, AMPA, DNQX, MK-801, nitrazepam, donepezil, and ondansetron were purchased from WAKO Pure Chemicals; ifenprodil, Ro25-6981, DL-AP7, felbamate, and loperamide were obtained from Sigma-Aldrich (St. Louis, MO, USA).

4.3. mRNA Analyses

Total RNA was prepared from the cerebellar hemispheres of 12-week-old mice (male and female) using the EZ1-RNA purification kit (Qiagen, Venlo Park, The Netherlands). For microarray analyses, GeneChip Mouse Genome 430A (Affymetrix, Santa Clara, CA, USA) was used, and differences in transcript levels were calculated with Partek (Partek Inc., St. Louis, MO, USA). The original data files (CEL-files) were deposited in the Gene Expression Omnibus (GEO) repository and assigned the GEO accession numbers: GSM1334015, GSM1334016, and GSM1334017 for normal mice, and GSM1334018, GSM1334019, and GSM1334020 for mutant mice. PCR primers for real-time PCR were as follows: *mGrid2* F, 5'-AAC ACG CTA CAT GGA CTA CTC-3' and *mGrid2* R, 5'-GAA GCA CTG TGC CAG CAA TG-3'; m*Gapdh* F, 5'-ACT CAC GGC AAA TTC AAC GG-3' and m*Gapdh* R, 5'-GAC TCC ACG ACA TAC TGA GC-3'. To amplify the *Grid2* ORF, primers are mGrid2 F2 (5ATG): 5'-ATG GAA GTT TTC CCC TTG CTC TTG T and mGrid2 R (3Stop): 5'-TCA TAT GGA CGT GCC TCG GTC GGG GTC A were used.

4.4. Measurements of Walking Distance and the OKR

Male mice (12–14 weeks old) were placed in a rectangular box (25 cm × 40 cm), and their head position was tracked for 5 min using ANY-maze software (Brain Science Idea, Osaka, Japan). Each mouse was monitored three times, and the longest distance recorded was used in the data analysis.

The OKR was measured in adult mice using previously described methods [28], which are depicted in Supplementary Figure S1. Briefly, the mice were anesthetized with isoflurane (2%) and a stainless steel screw was glued to the skull. The mice were then habituated to the experimental conditions for 2 days before the measurement. Ten minutes before the measurement were made, mice were administered a saline (8 mL/kg) injection with or without memantine (10 mg/kg) intraperitoneally. The mouse was then mounted on a stereotaxic apparatus and exposed to continuous sinusoidal horizontal oscillations (17°, 0.25 Hz) of a cylindrical checkerboard-patterned screen (diameter, 65 cm; single

square, 1.8 × 1.8 cm; brightness, ~30 lx). Right eye movement was captured at 30 Hz with an infrared camera. For each image frame, we used a machine vision system to estimate the pupil azimuth from the location of the pupil center. The OKR was expressed on a time plot of the relative pupil azimuth for each round of screen oscillation, with the pupil azimuth at the beginning of backward eye movement set to 0°. An OKR gain was defined as the ratio of the maximal relative pupil azimuth change to that of the screen (17°).

4.5. Cell Culture and Electrophysiology

Granule cell-enriched cultures were prepared as previously described [61]. Briefly, 2-day-old (P2) mutant or WT mice were anesthetized by cooling and then sacrificed by decapitation. The cerebella were dissociated with trypsin, plated on poly-L-ornithine-coated plastic dishes (Becton Dickinson, Franklin Lakes, NJ, USA) at 1.25 million cells/mL, and maintained in low-serum, nutrient-supplemented Dulbecco's Modified Eagle Medium/F-12 (Life Technologies; 5% CO_2, 37 °C) for 12 days.

Ruptured-patch whole-cell recordings were performed on cultured granule cells. The pipette solution contained 134 mM potassium D-gluconic acid, 7.6 mM KCl, 9 mM KOH, 10 mM NaCl, 1.2 mM $MgCl_2$, 4 mM ATP magnesium salt, 10 mM HEPES, and 0.5 mM EGTA (pH 7.3). The culture dish was perfused at a rate of 1.4 mL/min with 145 mM NaCl, 5 mM KCl, 2 mM $CaCl_2$, 10 mM HEPES, 10 mM D-glucose, and 10 μM glycine (pH 7.4). Current signals were recorded using an EPC-8 amplifier (holding potential, −90 mV; cut-off frequency, 5 kHz; sampling rate, 20 kHz; HEKA, Lambrecht/Pfalz, Germany) controlled by Patchmaster software (version, 2.35; HEKA). The command potentials were corrected for a liquid junction potential between the pipette and bath solutions. Electronic capacitance cancellation and series resistance compensation were not used. The series resistance (33.2 ± 5.1 MΩ, n = 55) and membrane capacitance were estimated from the amplitude and time constant of the capacitive current evoked by a 10 mV voltage jump. The bath solution containing 20 μM NMDA or 10 μM memantine was locally applied to the cell through a theta tube under the control of gravity and electromagnetic valves (VM8, ALA Scientific Instruments, Farmingdale, NY, USA). The magnitude of an NMDA-induced current was quantified as the inward current charge over a 2 s NMDA application normalized to the membrane capacitance (charge density). The background charge was estimated from a 0.5 s pre-application period and subtracted from the charge density.

4.6. Statistical Analyses

Data from each group were characterized by the mean ± SD, unless otherwise stated. Data from biochemical assays were examined with one-way ANOVA followed by unpaired two-tailed *t*-tests to detect statistically significant differences. All the statistical examinations were performed using JMP software (versions 9.0.2 and 10.0.1, SAS Institute, Cary, NC, USA).

Acknowledgments

We thank Junko Morita for her technical assistance and Takayoshi Imazawa for their kind advice. We thank Sebnem Kesaf and Ryuichi Shigemoto for their advice on performing OKR measurements.